ChemPubSoc Europe
DOI: 10.1002/cctc.201500662
CHEMCATCHEM
Full Papers

Onion-Like Graphene Carbon Nanospheres as Stable Catalysts for Carbon Monoxide and Methane Chlorination

Gabriele Centi,*[a] Katia Barbera,[a] Siglinda Perathoner,*[a] Navneet K. Gupta,[b] Erika E. Ember,[b] and Johannes A. Lercher*[b]

Thermal treatment induces a modification in the nanostructure of carbon nanospheres that generates ordered hemi-fullerene-type graphene shells arranged in a concentric onion-type structure. The catalytic reactivity of these structures is studied in comparison with that of the parent carbon material. The change in the surface reactivity induced by the transformation of the nanostructure, characterized by TEM, XRD, X-ray photoelectron spectroscopy (XPS), Raman, and porosity measurements, is investigated by multipulses of Cl_2 in inert gas or in the presence of CH_4 or CO. The strained C–C bonds (sp^2-type) in the hemi-fullerene-type graphene shells induce unusually strong, but reversible, chemisorption of Cl_2 in molecular form. The active species in CH_4 and CO chlorination is probably in the radical-like form. Highly strained C–C bonds in the parent carbon materials react irreversibly with Cl_2, inhibiting further reaction with CO. In addition, the higher presence of sp^3-type defect sites promotes the formation of HCl with deactivation of the reactive C–C sites. The nano-ordering of the hemi-fullerene-type graphene thus reduces the presence of defects and transforms strained C–C bonds, resulting in irreversible chemisorption of Cl_2 to catalytic sites able to perform selective chlorination.

Introduction

Carbon has been widely used as a support material for metal nanoparticles, particularly for hydrogenation reactions,[1] but recently the possibility to use carbon directly as a catalyst has emerged as an interesting option.[2–4] The catalytic performances of carbon materials depend on their nanoscale structure[5–7] as well as on the presence of functional groups, both of these aspects are reliant on preparation, doping, and functionalization.[2,3] Significant advances have been made recently in this direction for nanocarbon materials such as carbon nanotubes (CNTs), graphene, fullerene, and other nanocarbon catalysts (including fibers, coils, and horns, among others).[8,9] However, onion-type carbon materials, owing to their intrinsic more complex structure and the presence of different types of sites, remain less understood, although there is some relevant progress in this area.[10] Critical aspects to be further analyzed include the role of nano-ordering and the formation of fullerene-type nanostructures. Thermal annealing allows an increase in the degree of ordering (graphitization) and it may be possible to create fullerene-type nanostructures, depending on the nature of the starting carbon.

Although research on the catalytic properties of nanocarbon materials, such as CNTs and graphene, is increasing exponentially,[11–16] the catalytic use of onion-type carbon materials is largely unexplored. These materials may be visualized as hemi-fullerene-type graphene shells arranged in a concentric onion-type layered structure.[11] It is known that the strain of C–C (sp^2-type) bonds may activate the reactivity owing to the curvature present in these nanostructures, enabling coordination and activation of reactants ranging from O_2 to Cl_2.[3,11] Therefore, these structures have, in principle, interesting catalytic properties, which may be tuned by nano-ordering and suitable control of the parent amorphous carbon material, which in contrast, does frequently not show such catalytic properties.[17]

In general, the unique catalytic features of nanocarbons are derived from their atomic arrangement, that is, from their linear, trigonal, planar, or tetrahedral geometries,[18] and the presence of sp., sp^2-, and sp^3-hybridized carbon bonds.[19,20] In addition, the presence of surface strains, point defects, dangling bonds, and curvatures further enhances the catalytic performance.[21,22] Onion-like structures combines several of these features,[23–26] making it difficult to identify and characterize the specific sites responsible for a particular catalytic behavior. It has been suggested that the “surface roughness” influences the reactivity of onion-like carbon materials, facilitating redox reaction and desorption of reaction products, but more precise indications have not been provided.[24,27,28]

---

[a] *Prof. G. Centi, Dr. K. Barbera, Prof. S. Perathoner*
Department of Industrial Chemistry
and Engineering of Materials and CASPE-INSTM
University of Messina
98166 Messina (Italy)
E-mail: centi@unime.it
perathoner@unime.it

[b] *Dr. N. K. Gupta, Dr. E. E. Ember, Prof. J. A. Lercher*
Technische Universität München
Department Chemie
Lichtenbergstr. 4, 85747 Garching (Germany)
E-mail: johannes.lercher@mytum.de

Supporting Information and ORCID(s) from the author(s) for this article are available on the WWW under http://dx.doi.org/10.1002/cctc.201500662.

This publication is part of a Special Issue on Carbon in the Catalysis Community. Once the full issue has been assembled, a link to its Table of Contents will appear here.

© 2015 Wiley-VCH Verlag GmbH & Co. KGaA, Weinheim

The presence of curvature and strains in C–C bonds may activate adsorbed reactants and decrease the activation energy, but it is not known whether the activation leads to irreversible chemisorption or is effective in promoting catalytic reactions. It may be expected that the nano-ordering induced by thermal treatment of carbon materials, which are precursors to surface nano-onion-type structures, can thus provide a useful approach to understand this problem, and at the same time provide a way to create specific catalytic sites. In the presence of disordered nanostructures, carbon is more reactive at the edges, which have lower bond energies ($\approx 7\,\mathrm{kcal\,mol^{-1}}$), and usually result in irreversible reactions with adsorbed reactants. More ordered carbon nanostructures have a larger energy barrier for chemisorption, but would allow, in principle, the transformation of stoichiometric chemisorption sites into catalytic sites.[2]

It has to be remarked that the catalytic behavior of strained C–C (sp^2-type) bonds is still largely unexplored. In nanocarbon materials, such as graphene and CNTs, which have been extensively studied from the catalytic perspective,[3] the reactive sites are associated essentially to edges or defects. Fullerenes, owing to the curvature of C–C sp^2-type bonds, are known to readily react with various bi-atomic molecules, but in a stoichiometric way only.[11] The possibility of the utilization of these reactive sites for the catalytic activation of small bi-atomic molecules is thus highly challenging. Nano-onion-type carbon materials have a high presence of strained C–C sites, and the tuning of their characteristics is also possible. From a catalytic perspective, therefore, these materials have the potential of being of high interest, especially when combined with a low-cost preparation method, as is described herein.

As a reaction to probe the surface chemistry, the catalytic activation of Cl_2 is used. This reaction is relevant to understand the utilization of these catalysts in chlorination reactions, for example, the synthesis of chloroform from methane or the synthesis of phosgene from CO; two structure-dependent reactions realized on large scale (about 5–6 Mtons/y).[29,30] Phosgene is produced industrially by catalytic chlorination of CO, a strongly exothermic reaction.[31–33] The formation of byproducts (hydrochloric acid, and carbon tetrachloride[34]) depends strongly on the type of activated carbon catalysts used in the process. In fact, the extensive chlorination of the carbon material leads to weakening of the carbon–carbon bond and the formation of gas-phase chlorination products, with a concomitant loss of catalyst material and a decrease of the available active sites. The gas-phase chlorinated hydrocarbons can further polymerize in the gas phase and form high-molecular byproducts, which readsorb onto the surface and deactivate the catalyst by blocking the active sites. Therefore, the carbon properties have to be optimized to minimize both HCl and CCl_4 formation, as well as irreversible chlorine adsorption, while maintaining as high a rate as possible for phosgene synthesis.[35,36] Although the reaction of graphene-type materials with chlorine atoms has been previously reported,[37–40] results on the uptake, rather than on the catalytic behavior, have not been shown. In addition, the dependence of these properties on the nanostructure is unclear.

The selective synthesis of halogenated compounds from CH_4 over carbon catalysts helps to understand the radical chemistry of Cl_2. It should be noted that there is great interest in the conversion of methane to olefins and gasoline by mono-halogen alkanes, as an alternative route to methanol conversion.[41–45] Carbon materials offer an interesting alternative to metal oxides, which may form volatile halogenides[46] and have problems with long-term stability related to the volatility of $MeCl_x$ species.

In previous work[47,48] we have shown a method to obtain carbon nanospheres characterized by stacks of sp^2-graphene-like nanosheets starting from an amorphous carbon obtained by the controlled pyrolysis of glucose. These materials showed an onion-like carbon structure, that is, spherical closed carbon graphene shells arranged in a concentric layered structure, resembling that of an onion.[49–51] Following the acronym suggested by Zhang et al.[52] we indicated these materials as onion-like carbon nanospheres (OCNSs). The resulting material shows high surface area and a structural order in the stacking of the graphitic layers. These results evidence the possibility to prepare different types of nanostructure sp^2–sp^3-mixed-carbon systems, with different degrees of nano-ordering. The aim of this work is to compare two carbon nanomaterials with an analogous nanostructure, but a different degree of ordering, in the reaction with Cl_2, CO, and CH_4. The combined experiments help to understand how the local nanostructures influence the surface reactivity.

Results and Discussion

Physicochemical characterization

TEM micrographs of CHT and CHT-tr samples (see definition in the Experimental Section, Synthesis) are shown in Figure 1. It should be noted that we have previously studied similar samples.[47] Although the samples reported here were prepared again choosing optimized conditions, the results are similar, confirming the reproducibility of the preparation. The hydro-

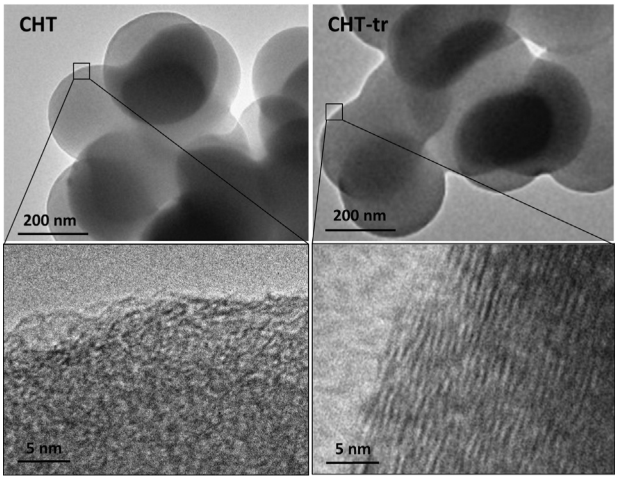

Figure 1. TEM images of CHT and CHT-tr catalysts at different magnifications.

thermal procedure used to prepare the CHT sample gives rise to a uniform distribution of spherically shaped carbon nanoparticles, with an average main diameter in the 200–400 nm range. After thermal annealing, the spherical shape and morphology is almost retained, although a different degree of ordering is shown by TEM characterization (Figure 1). CHT-tr shows the presence of a graphitic-like structure, with a characteristic nano-onion rearrangement, initiating at the surface and propagating inside the nanoparticles, forming concentric shells of C sp^2-bonded atoms from the spherical or cylindrical shape of the original amorphous precursor.

Table 1. Crystallographic parameters (from XRD measurements) of CHT and CHT-tr (see text for description).

Sample	d_{002} [nm]	L_a [nm]	L_c [nm]	L	G_I (LiF as reference)	relative G_I (100 % for CHT-tr)
CHT	0.376	–	0.79	–	5.5	27.3
CHT-tr	0.349	4.5	1.04	0.34	20.1	100

The crystallographic parameters determined by XRD patterns for CHT and CHT-tr samples are reported in Table 1. The calculated d_{002} spacing for CHT-tr was 0.349 nm, suggesting the formation of a quasiordered graphitic layer, although with larger interlayer spacing (d_{002} for graphite is 0.335).This d_{002} value is significantly larger in the CHT sample, owing to the presence of a highly disorganized situation. In CHT the (110) reflection is so weak, that it does not allow an estimation of L_a (basal plane length), and as consequence, L (effective dimension of graphitic microcrystallites, see the Supporting Information). The L_c (height of layered stacking, see the Supporting Information) value indicates the presence of some ordering along this crystallographic direction, but not in the orthogonal direction, as expected from a disordered organization, characteristic for the precursor of an onion-type nanostructure. This indication is in agreement with the TEM data (Figure 1).

Table 2. Textural properties of the samples. Surface area determined by BET and Langmuir methods, area of the micropores, total pore volume, and volume of micropores.

Sample	SA_{BET}–SA_{Lang} [m^2 g$_{cat}$$^{-1}$][a]	Micropore area[b] [m^2 g$_{cat}$$^{-1}$]	Total pore volume [cm^3 g$_{cat}$$^{-1}$]	Micropore volume[b] [cm^3 g$_{cat}$$^{-1}$]
CHT	635–840	503	0.31	0.23
CHT-tr	585–770	550	0.26	0.25

[a] SA = Surface area. [b] determined by t-plot method.

The textural characteristics of the CHT and CHT-tr samples have been determined by nitrogen sorption isotherms (Table 2). The CHT sample has a very high surface area (≈640 m^{2}g$_{cat}$$^{-1}$) with a major contribution of the micropore fraction (≈500 m^{2}g$_{cat}$$^{-1}$). Upon annealing in N_2 at 1000 °C for 6 h, there is a decrease both in surface area and pore volume (−20 and −16 %, respectively), with a corresponding increase in the microporosity (≈10 %). This increase in microporosity after annealing is surprising, because typically microporosity decreases. One explanation could be the presence of hydrocarbon impurities in the carbon micropores, filling the micropores and making them inaccessible during the determination of the microporosity. The desorption of these adsorbed organic species during the annealing procedure would thus lead to the apparent increase of the microporosity. However, thermogravimetric (coupled with mass spectrometer analysis of the gas evolution) and FTIR data on similar samples[47] also shows an increase of the microporosity after annealing, excluding that the increase of microporosity is related to desorption of the organic species present in the carbon micropores. Therefore, we may conclude that the effect is related to a structural reorganization, which is consistent with the TEM and XRD results and previous literature indications.[53–56]

Raman spectroscopy illustrates further the differences between the CHT and CHT-tr samples (Figure 2). CHT shows a broad fluorescence background, which could be due to the presence of organic impurities and/or surface defects. The thermogravimetric data cited above indicates the absence of significant organic adsorbed species, but does not allow the presence of traces of adsorbed species, enough to give the fluorescence effect, to be excluded. However, it is likely that the fluorescence is related to the strongly defective situation, as indicated by TEM data. It is known that strong fluorescence originates in nanocarbon materials from the electronic transitions among/between the nonoxidized carbon regions and the boundary of oxidized carbon atom regions, where different functionalized groups C–O, C=O, and O=C–OH are present.[57] This is in agreement with the indication by EDS that the amount of oxygen in CHT is approximately 10 %.

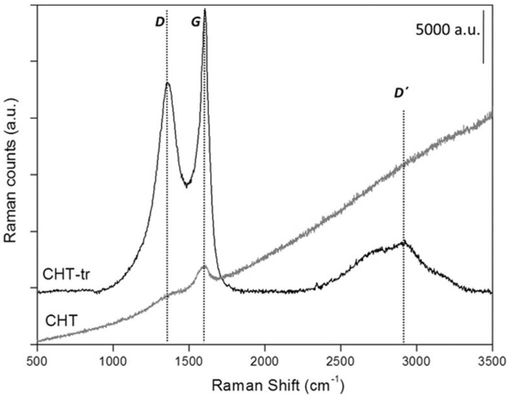

Figure 2. Raman spectra of CHT and CHT-tr.

The Raman spectrum of CHT-tr exhibits two main bands at 1586 and 1344 cm^{-1}. These bands are also present in the CHT sample, but are broader and weaker. The G (1580–1600 cm^{-1}) and the D (1350 cm^{-1}) peaks are usually assigned to zone center phonons of E_{2g} symmetry and K-point phonons of A_{1g}

symmetry, respectively. They can be attributed to many forms of sp^2-bonded carbons with various degrees of graphitic ordering, ranging from microcrystalline graphite to amorphous carbon.[5] The *G* peak involves the in-plane bond-stretching motion of pairs of all sp^2 sites (not necessarily only those arranged in six fold rings). However, the *D* peak is forbidden in perfect graphite and becomes active in the presence of a more disordered structure.[54–56] The intensity ratio between these two bands (I_D/I_G) is usually indicative of the relative degree of disorder.[53] In the case of CHT-tr, the I_D/I_G is equal to 0.77. According to the Tuinstra and Koenig equation:[58]

$$\frac{I_D}{I_G} = \frac{C(\lambda)}{L_a} \tag{1}$$

a correlation between the I_D/I_G ratio and the L_a value obtained from XRD measurements exists. In our case, the values lie within the range where I_D/I_G is proportional to $1/L_a$, analogous to the case of graphite or nanocrystalline graphite with uniform crystallization (see S3 and Table S1, in the Supporting Information).[53,54] It should be noted that some authors have argued that the absolute intensity of the *G* band may be a more suitable parameter than the *D*/*G* ratio.[59,60] However, this estimation requires a more complex procedure, for example, measuring the *G*-band intensity of liquid suspensions of single-walled CNT (SWCNT) samples as a function of solid concentration.[60] This procedure is necessary to quantify the purity of SWCNT, but is not necessary to have an indication of the degree of disorder, as in our case.

The presence of oxygen functionalities in CHT and CHT-tr was analyzed by X-ray photoelectron spectroscopy (XPS) measurements of C_{1s} and O_{1s} signals. The C_{1s} spectra of CHT and CHT-tr are shown in Figure 3. CHT shows a right shoulder in comparison with the sharp and symmetric graphitic C_{1s} peak present in CHT-tr, probably because of the removal of functional C–OH, C=O, and COOH groups[61] during the annealing process. The main C_{1s} peak shifts from approximately 283.8 eV in CHT to 282.7 eV in CHT-tr, which is consistent with the change from a prevalent sp^3 to a sp^2 configuration after thermal annealing.[54] The transformation during the annealing process is confirmed by the analysis of the O_{1s} region (Figure 3), presenting a main peak centered at 530.03 eV with a right shoulder centered at approximately 533 eV, which disappears after thermal annealing. This shoulder position is consistent with that expected for –COOH-type surface species, whereas that at around 530 eV is typical for quinones and C=O species, which are known to be thermally more stable than –COOH-type oxygen functional groups present in carbon materials.[5]

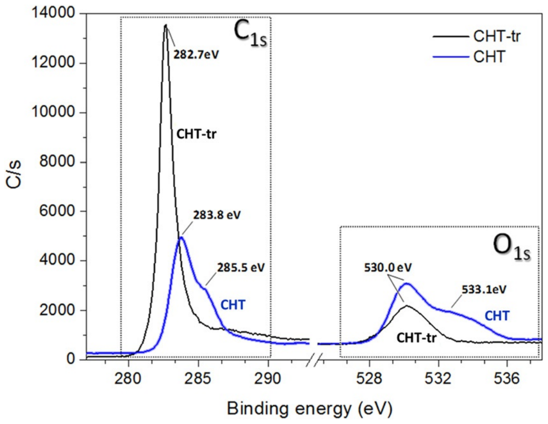

Figure 3. XPS of C_{1s} and O_{1s} for CHT and CHT-tr.

Catalytic reactivity

Reversible and irreversible Cl_2 uptake by CHT and CHT-tr

The surface reactivity of CHT and CHT-tr towards Cl_2 was studied by a sequential multipulse method at 200 °C. HCl was the only product observed in the reactor outlet stream, in addition to Cl_2. From the difference of Cl_2 content in the inlet and outlet streams, the amount of reacted Cl_2 can be determined. By subtracting the HCl formed, it is possible to determine the amount of irreversibly chemisorbed Cl_2. In addition, from the difference in the peak shape of the single Cl_2 peaks, with respect to those observed when the catalyst is absent, an indication of the type of reversible chemisorption of Cl_2 can be deduced.

Typical profiles recorded during Cl_2 sequential pulses on CHT and CHT-tr are shown in Figure 4a and 4b, respectively. HCl is the major product formed initially, up to approximately 3000 s for CHT and approximately 1500 s for CHT-tr. Cl_2 starts to be detected when the formation of HCl begins to end. However, the formation of HCl does not correspond to the total amount of converted Cl_2. From the amount of Cl_2 converted and that of HCl detected in the gas phase, the total irreversible Cl_2 uptake is calculated (Table 3). The amount of irreversible uptake of Cl_2 by CHT is three times higher than the amount calculated for CHT-tr. Similarly, HCl formation is ≈2–3 times higher in CHT with respect to that in CHT-tr. After approximately 6000 s, the Cl_2 pulse intensity at the reactor outlet reaches an intensity almost corresponding to the inlet value. It should be noted that the formation of HCl requires the presence of H-donor species on carbon sites near to those of chlorine activation, as discussed in a more detail below.

Table 3. Cl_2 multipulse experiments on CHT and CHT-tr at 200 °C in continuous He flow. Experimental error in the ±5–10% range.

Sample	Irreversible Cl_2 uptake [$mmol\,g_{cat}^{-1}$]	HCl formation [$mmol\,g_{cat}^{-1}$]
CHT	7.36	9.70
CHT-tr	2.16	3.90

The difference in peak shape between the inlet and outlet Cl_2 pulses, as a consequence of the interaction of Cl_2 with the catalyst, provides further interesting indications. For the CHT

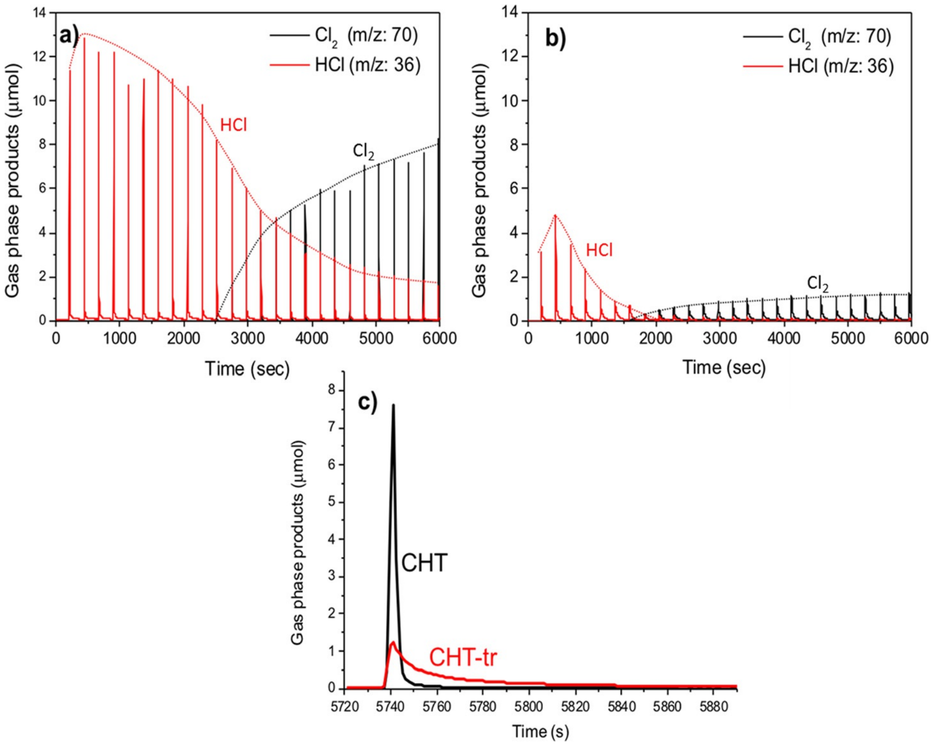

Figure 4. Cl_2 multipulse experiments on a) CHT and b) CHT-tr in He continuous flow. c) Comparison of the reactor outlet Cl_2 pulses for CHT and CHT-tr. Experimental conditions: 30–50 Cl_2 pulses (230 s pulse length) (3.6 μmol Cl_2/pulse), He flow: 10 mL min^{-1}, 10 mg of material, $T = 200$ °C.

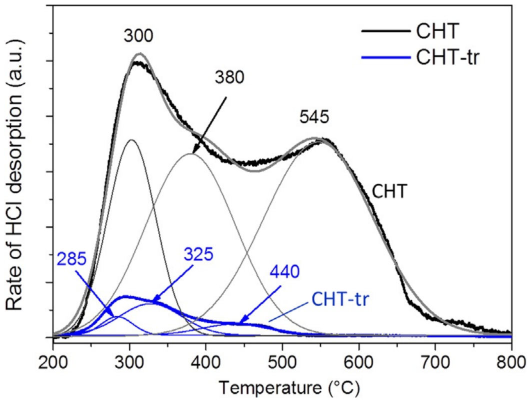

Figure 5. Temperature-programmed desorption of CHT and CHT-tr after exposure to multiple pulses of Cl_2 (6000 s, experimental conditions as in Figure 4).

catalyst the difference is minor and the peak remains sharp (Figure 4c), however, a greater difference is noted for CHT-tr, which shows a long tail. This finding indicates an unusually strong, but reversible, interaction of Cl_2 with the more ordered catalyst. Therefore, CHT-tr is characterized by a high amount of reversible adsorption of Cl_2, whereas CHT shows a high irreversible uptake of Cl_2, as well as higher formation of HCl.

After equilibration with Cl_2 at 200 °C (e.g. after 6000 s), the temperature of the catalyst was increased linearly [temperature-programmed desorption (TPD) experiments] to analyze the type of surface species present on the catalyst (Figure 5) and their energy of interaction with the catalyst. Both CHT and CHT-tr show a very broad, structured desorption profile of HCl between 200 and 800 °C. The total amount of HCl (8.2 mmol g^{-1}) desorbing at three different temperatures (300, 380, and 545 °C) from CHT was approximately 14 times higher than in the case of CHT-tr (0.6 mmol g^{-1}). For both catalysts, no other chlorinated species were detected during the TPD experiments. Also, the CHT-tr sample shows three desorption peaks, but with maxima shifted to lower temperatures (285, 325, and 440 °C) and the peak relative to the intermediate temperature becoming more intense. These results confirm that thermal treatment not only induces a strong decrease of the sites responsible for HCl chemisorption, but also a slight change in their nature.

However, it could be suggested that the three peaks correspond to three types of chemisorbed HCl species with different energy of interaction, with the surface sites, or maybe a different interpretation is possible. Part of the discussion, which will be more extensive later, is that HCl is derived from the reaction of Cl atoms produced by dissociative chemisorption of Cl_2 and H-donor sites, related to defective sp^3-type C atoms. When these sites are located near to a Cl atom coordinated to carbon, desorption of HCl may occur. Otherwise, a surface migration of hydrogen atoms to the carbon atom coordinating Cl could occur, and HCl may form and desorb. The three observed peaks for HCl desorption in the TPD experiments after the multipulse of Cl_2 (Figure 5) may be, therefore, alternatively interpreted as deriving from three different energy paths necessary for surface diffusion of the hydrogen to reach the carbon atom coordinating Cl. It should be also recalled that neither on CHT nor CHT-tr samples is desorption of Cl_2 detected during TPD experiments. Therefore, all chemisorbed (intact) Cl_2 desorbs reversibly at 200 °C (even if the peak-shape analysis discussed above evidences the presence of a strong chemisorption on CHT-tr), whereas dissociative chemisorbed Cl_2 requires higher temperatures for desorption. The ability to explain why this occurs could lead to progressive catalyst deactivation.

The structural changes on the active sites of CHT-tr, caused by Cl_2 treatment, were monitored by in situ Raman spectroscopy. Raman spectra recorded during the interaction of Cl_2 with CHT-tr (Figure 6) show that after a short time of Cl_2 exposure (3 min) both *D* and *G* bands decreased in intensity, indicating

© 2015 Wiley-VCH Verlag GmbH & Co. KGaA, Weinheim

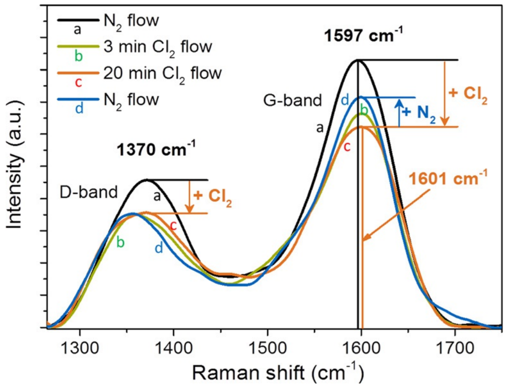

Figure 6. In situ Raman spectra of CHT-tr in contact with Cl_2 at 40 °C.

a marked interaction of sp^3- and sp^2-hybridized carbons with adsorbed Cl_2. On increasing the time of exposure, the *D* band does not change further, whereas the *G*-band intensity continued to decrease. The *D*-band intensity was not affected when the Cl_2 stream was replaced with N_2, whereas the *G* band recovered part of the intensity, indicating the reversibility of the adsorption processes on Cl_2 in CHR-tr, according to the results reported in Figure 4. As commented before, the *D* band is a second-order Raman scattering process that is enhanced by the presence of defects, whereas the G band involves the in-plane bond-stretching motion of pairs of all sp^2 sites. These in situ Raman results thus indicate that defect sites (sp^3-like) irreversibly interact with Cl_2, whereas C–C bonds (sp^2-type) can give reversible chemisorption of Cl_2. However, pure graphene does not interact with Cl_2 (except at the edges), neither is it active in phosgene generation, and the highly strained C–C bonds in fullerene give only irreversible dissociative chemisorption.[62,63]

Reactivity of the surface chlorine species

The reactivity of surface chlorine species in the two catalysts was studied by multipulse Cl_2 experiments in the presence of a continuous flow of He–CO (5 vol% CO) or He–CH_4 (5 vol% CH_4).

CO as a probe molecule

The reactivity of chemisorbed chlorine species towards CO was investigated by sending pulses of Cl2 while continuously feeding a mixture of 5 vol% CO in He over the catalyst. The results for the CHT and CHT-tr catalysts are reported in Figure 7. The presence of CO in the feed (Figure 7) modifies significantly the behavior with respect to the similar tests, where instead an inert gas only was fed together with Cl_2 (Figure 4). Cl_2 starts to be detected in the reactor stream after approximately 2000 s for CHT, but is not detected for CHT-tr, which is different to the case without CO. The irreversible Cl_2 uptake was estimated to be 10.5 and 3.7 mmol g^{-1} for CHT and CHT-tr, respectively. These values are slightly higher than those measured in the absence of CO (Table 3), but the difference is within experimental error, which can be estimated in the range of ±5–10%.

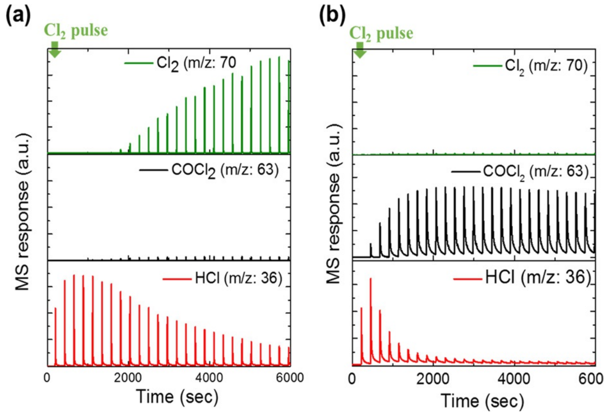

Figure 7. Cl_2 multipulse tests at 200 °C on a) CHT and b) CHT-tr in He/CO (5 vol.% CO) continuous flow. Experimental conditions as in Figure 4.

In fact, the ratio of the irreversible Cl_2 adsorption of CHT with respect to that of CHT-tr remained almost constant at, for example, approximately threefold. We may conclude that the concentration of irreversibly adsorbed Cl_2 remains almost identical in the presence and absence of CO, indicating that the reaction of the irreversible chlorine chemisorbed species with CO does not occur.

Although $COCl_2$ does not form on the CHT catalyst, a significant amount of $COCl_2$ is detected with the CHT-tr catalyst. For CHT-tr, there is an initial delay in $COCl_2$ formation, which starts when HCl formation ends. On the contrary, much more HCl formation is detected for CHT. It is worth noting that the formation of HCl passes through a maximum for both catalysts, suggesting that the mechanism of formation of HCl involves first the dissociative chemisorption of Cl_2 and then the reaction of the formed species with the H-donor species, thus generating HCl. Note also that TPD experiments allowed the exclusion of chemisorbed water or hydrocarbons over the catalysts surface and, therefore, these H-donor species are those associated to sites present on the catalyst.

The conversion of Cl_2 and the formation of $COCl_2$ on the CHT and CHT-tr catalysts and the relative graphitization index (G_I), that is, the graphitic degree in respect to the CHT-tr sample (set equal to 100%), are summarized in Figure 8. G_I

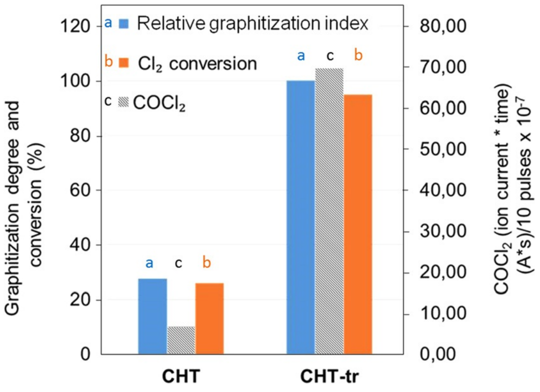

Figure 8. Relationship between graphitization degree, Cl_2 conversion, and $COCl_2$ formation on CHT and CHT-tr.

characterizes the transition from sp^3 to sp^2 carbon and the formation of the onion-like structure.

CH_4 as a probe molecule

To explore the radical nature of the chemisorbed chlorine species, their reactivity with CH_4 was investigated over both a CHT-tr sample and in an empty reactor, as reference. The results obtained are summarized in Figure 9. The reaction, known to occur with radical-type chlorine species,[64] was conducted at 200 °C pulsing Cl_2 in a continuous flow of He and CH_4 (5 vol %), and under dark conditions (light may promote the halogenation). Halogenated methane species, CH_3Cl, CH_2Cl_2, $CHCl_3$, and CCl_4, are the products of the reaction, with a distribution consistent with the presence of radical-type chlorine species on the surface of the catalyst. These products were also observed without the catalyst (in the empty reactor), albeit in minor amounts, and were considered in the evaluation of the catalyzed reaction. The fact that the distribution of the products, however, does not significantly change in the tests with and without the catalyst is in accordance with the radical-type mechanism and proves that the onion-type catalyst was active in producing chlorine-radicals, which reacted with methane to give chloromethanes with a distribution in agreement with that expected for radical-type reactions.

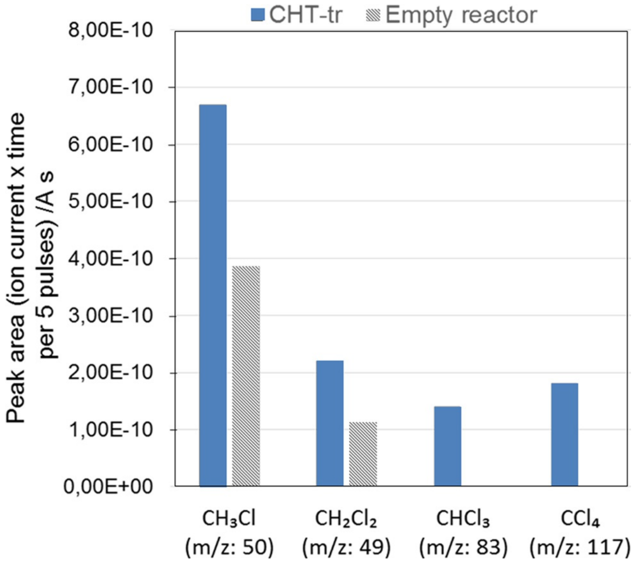

Figure 9. Total amount of CH_3Cl, CH_2Cl_2, $CHCl_3$, and CCl_4 formed in 6000 s during Cl_2 multipulse experiments at 200 °C in an empty reactor and in the presence of CHT-tr under continuous He/CH_4 (5 vol % CH_4) flow. Experimental conditions as in Figure 4.

Nature of the reactive sites

Overall, spectroscopic, structural characterization, and kinetic measurements show that the thermal treatment creates a unique carbonaceous species, a nanoscopically defined hemi-fullerene-type structure. The combination of the layered carbon structure and the specific bending of the hemisphere create highly active sp^2-hybridized carbon atoms, which are proposed to be the site responsible for Cl_2 reversible activation. Carbon-terminating defects (sp^3 hybridized) are responsible for irreversible chemisorption, similar to highly strained C–C bonds. Raman in situ experiments (Figure 6) support this conclusion, and tests with methane as a probe molecule suggest a radical-like character of this reversibly chemisorbed (undissociated) Cl_2 species.

The results reported in Figure 4 and 7 show that CHT and CHT-tr differ in terms of reversible and irreversible uptake of chlorine species on the surface. Cl_2 uptake was mainly irreversible in CHT, whereas CHT-tr shows less irreversible chemisorption (as well as HCl formation) and the presence of a reversible chemisoption, although with strong interactions with carbon surface sites. Based on previous comments, Raman and other characterization results, it is reasonable to attribute the sites able to reversibly activate Cl_2 to moderately strained C–C bonds (sp^2-type). Nano-ordering during thermal treatment induces the conversion of sites with irreversible (dissociative) chemisorption of Cl_2 to sites that chemisorb Cl_2 strongly, but in a molecular (reversible) form. Dissociatively chemisorbed Cl_2 may then react with surface H-donor sites to generate HCl. The formation of the HCl, therefore, requires the presence of H-donor sites. TPD data excludes the presence of possible hydrogen donor species, such as water or hydrocarbons adsorbed on the carbon surface, therefore, these H-donor species are associated to hydrogen atoms saturating the carbon defects, or are present as –OH or –COOH surface groups.

Catalyst characterization data show that these H-donor sites may be associated to sp^3 carbons at defect sites (carbon-terminating sites). When these H-donor sites are no longer available, CO reacts with molecular chemisorbed Cl_2, leading to $COCl_2$. However, although the HCl maximum formation in CHT is detected at approximately 1000 s, $COCl_2$ formation is not detected over this catalyst, at least up to 6000 s. This finding suggests that desorption of HCl does not allow the restoration of the original active site and thus surface reactivity toward Cl_2 decreases progressively (Figure 7 a). Reasonably, this is due to the fact that the other Cl atoms derived from dissociative chemisorption of Cl_2 remain chemisorbed on the catalyst, blocking the active sites. Only at higher temperatures does the mobility of hydrogen on the surface allow the complete desorption of HCl, as shown from the TPD results (Figure 5). Data in Figure 4 c shows that sites that strongly chemisorb Cl_2, although still in a reversible molecular form, are present in CHT-tr, but not in CHT.

These observations may be rationalized by considering that different types of C–C (sp^2-type) bonds are present in the catalysts:

1) Highly strained C–C bonds, derived from disordered nano-onion-type structures that can irreversibly react with Cl_2, giving rise to homolytic dissociation of the Cl–Cl bond; these sites are similar to those present in fullerene-type

© 2015 Wiley-VCH Verlag GmbH & Co. KGaA, Weinheim

carbon materials and have a high bending (pyramidalization) degree and a similar irreversible uptake of Cl_2.[11,65–67]

2) Strained C–C bonds, derived from the nano-ordering process, are able to strongly chemisorb Cl_2, but in a molecular reversible form; these sites are responsible for $COCl_2$ formation, in presence of CO, and also promote CH_4 chlorination.

3) C–C bonds with moderate to weak strain do not interact, or have a weak interaction, with Cl_2.

Therefore, it is reasonable that HCl forms when H-donor sites, associated to defective sp^3-carbon sites, are present near to the first two types of sites. In such configurations, the other Cl atom (derived from Cl_2 dissociative chemisorption) remains strongly chemisorbed, but not in a position near to a H-donor site, thus resulting in the inhibition of that site. Nano-ordering that occurs during the thermal treatment leads to the elimination of these defect sites, in agreement with the significantly lower formation of HCl in CHT-tr compared to that in CHT. The larger formation of $COCl_2$ in CHT-tr originates from both the modification of the characteristics of C–C bond (sp^2-type) and the elimination of carbon defects (sp^3-type).

This indication is further supported from the data reported in Figure 8, in which Cl_2 conversion and $COCl_2$ formation on the two catalysts are compared with respect to the relative graphitization index. This index characterizes the transition from sp^3 to sp^2 carbon and thus the formation of the onion-like structure. This result gives further support to the above interpretation. However, further experiments are necessary for a better understanding of the unusually high strength of the interaction between Cl_2 and CHT-tr and the exact nature of these sites in the onion-type nanostructure. The relationship between HCl formation and the concentration/nature of defect sites in carbon also requires further clarification.

The irreversibly chemisorbed Cl_2 species, owing to their strong interaction, are not reactive towards CO, and are not in equilibrium with the reversibly chemisorbed species. This finding is consistent with the hypothesis that irreversibly adsorbed species are those that are homolytically dissociated (e.g. ClC–CCl), whereas those that are reversibly chemisorbed are molecular species. Thermal treatment, by inducing nano-ordering, minimizes the concentration of defects (sp^3-type carbon sites) and the amount of strongly bent C–C bonds (sp^2-type), limiting irreversible Cl_2 chemisorption and HCl formation. To further support this indication, Figure 10 reports the inverse correlation between the graphitization index (G_I) of the carbon atoms, the total amount of HCl formed, and the concentration of irreversibly chemisorbed Cl_2. Note that CHT-tr contains only one fourth of the sp^3 carbon atoms compared to the parent CHT. This is paralleled by an approximately four times lower Cl_2 uptake and HCl formation.

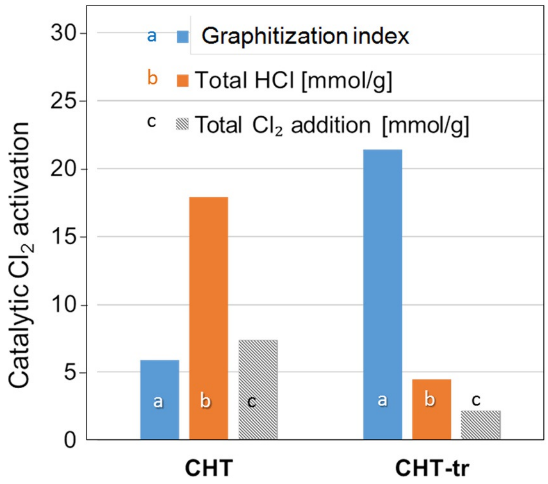

Figure 10. Relationship between the graphitization index (G_I) of carbon materials and the catalytic Cl_2 activation.

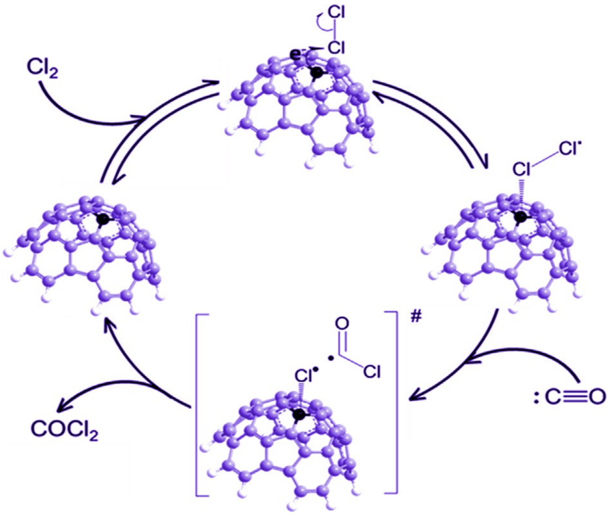

Scheme 1. Proposed $COCl_2$ synthesis mechanism on CHT-tr carbon materials.

Reaction mechanism

The tentative catalytic cycle for $COCl_2$ formation, which describes the experimental evidence discussed above, is presented in Scheme 1. Although in part speculative and deserving of further investigations, this proposal may be useful to analyze the discussed experimental results. During Cl_2 interaction with sp^2-carbon sites, labile charge-transfer complexes [$*C\cdots Cl_2$] are formed. Raman in situ spectra confirm this type of interaction, and reactivity data shows that when there is a relatively strong interaction, although reversible and involving undissociated Cl_2 molecules, a subsequent reaction with CO to form phosgene may occur. Following the subsequent charge transfer from carbon material to Cl_2, a new chlorine radical [$*C–Cl_2^{\cdot}$] species is generated that reacts with CO, forming $COCl_2$ via an acylchloride radical [${}^{\cdot}COCl$]. The presence of such a radical-like chlorine chemisorbed species is confirmed by the tests with CH_4 as probe molecule. In fact, the product distribution of methylchlorides is in agreement with the presence of radical-like species at the active carbon surface.

The key in the reaction mechanism is the type of carbon sites responsible for the first step of labile charge-transfer complex formation. According to the discussion in the previous section, C–C sp^2-type bonds are not active enough for this activation of Cl_2. Bending of the bond (strained C–C bonds) reduces the activation energy, allowing coordination and relatively strong chemisorption, although still in a reversible molecular form [Eq. (2 a)]. A higher bending degree (highly strained C–C sites), as present in more disordered onion-type materials and fullerene-type carbons, further decreases the activation energy, leading to dissociative chemisorption [Eq. (2 b)].

$$*C{=}C* + Cl_2 \rightarrow *C{-}C*(\cdots Cl_2) \tag{2a}$$

$$*C{=}C* + Cl_2 \rightarrow (Cl)*C{-}C*(Cl) \tag{2b}$$

Formation of HCl occurs either consecutively to the formation of dissociatively chemisorbed Cl_2 [Eq. (2 b)] by reaction with carbon sites with terminating defects (*C–H) [Eq. (3 a)] or alternatively by direct heterolytic chemisorption on these sites [Eq. (3 b)]. We believe that Equation (3 a) is more likely and is in better agreement with the experimental results, in particular with Raman data (Figure 6), however, this is an aspect deserving of further studies.

$$(Cl)*C{-}C*(Cl) + *C{-}H \rightarrow (Cl)*C{-}C* + HCl + *C \tag{3a}$$

$$*C{-}H + Cl_2 \rightarrow *C{-}Cl + HCl \tag{3b}$$

Generation of the active sites

The results show how two carbon samples, with almost identical round-shaped macroscopic morphology and similar surface area and porosity, change their reactivity towards Cl_2 activation and further catalytic CO and CH_4 chlorination by variation of their structural order.

By using thermal annealing, onion-type carbon nanospheres, with hemi-fullerene-type ordered nanoshells on the surface, have been prepared. The nanoshells are obtained by thermal reordering of the precursor, highly defective, carbon material, but possibly already have the suitable structure to form this specific surface nanostructure upon annealing. The catalyst obtained after the thermal treatment, with respect to the parent carbon material, has sp^2-carbon sites with unusually high strength for the adsorption of Cl_2 molecularly (in a reversible manner), leading to high catalytic activity in phosgene generation, significantly higher than for many other type of carbon materials (although not shown here). The annealing process lowers the amount of sp^3-type defect carbon sites, responsible for Cl_2 conversion to HCl. Possibly, the thermal ordering process, indicated by the increase of G_l, also causes modifications of highly strained sp^2-carbon sites responsible for irreversible Cl_2 chemisorption, although there is no definitive evidence on this aspect.

This special carbon nanostructure requires, to be created by thermal treatment, a suitable and specific carbon arrangement in the (quasi-amorphous) precursor. The synthesis of these precursor nanospheres depends not only on the precursors and the heat-treatment conditions, but also on the environment in which the carbon spheres are generated. In the case of CHT synthesis, the solid–liquid interface between the carbon source and the surrounding water during the thermal decomposition plays a key role in the concentric growth of the spherical carbon.[48] As for the macroshape, the nano-order in this material resembles that of nano-onion, but with a great disorder. The presence of sp^3–sp^2 mixed coordination, with the curvature process leading to nanospheres with a size of $\approx$200 nm, favors the formation of disordered stacking planes with various terminations and defects (sp^3-type carbon atoms). Thermal annealing, however, rearranges these layers into materials ordered at the nanoscopic level, according to the description outlined above.

Conclusions

A novel nanostructured carbon was synthesized by a combination of thermal decomposition in an aqueous environment and subsequent thermal annealing. This carbon material shows a unique strain on the graphene sheets, inducing carbon sites for strong chemisorption of Cl_2.

In the parent carbon material, the high degree of bending in C–C sp^2-type bonds induces irreversible dissociative chemisorption of Cl_2, and the high concentration of defect carbon atoms (sp^3-type, to which H atoms are coordinated to saturate the valence) favors further reaction of chemisorbed Cl species to generate HCl. Thermal annealing forms nano-ordered hemispherical graphene shell structures (hemi-fullerene type) with a decrease of the strain in C–C sp^2-type bonds, as well as a reduction of defect (sp^3-type) carbon atoms. The reorganization transforms sites able to irreversibly (dissociatively) chemisorb Cl_2 to sites able to strongly, but reversibly and in a molecular form, coordinate Cl_2. These sites react with CO to catalytically generate $COCl_2$, and also promote CH_4 chlorination. Reorganization also reduces the concentration of carbon defects (sp^3-type), thus decreasing HCl formation and catalyst deactivation.

During interaction with these sites, the formation of [$*C{-}Cl_2$] adducts with radical character is enabled. By using CO and CH_4 as reactive probe molecules, it was possible to show that this is the only species able to contribute to $COCl_2$ synthesis and $CH_{4-n}Cl_n$ formation. The properties and catalytic potential of this new material are currently being further explored.

Experimental Section

Experimental set-up and safety issues

One major advantage of the experimental setup designed for Cl_2 activation studies is the possibility to use minimal amounts of toxic and corrosive gases. A six-port valve connected to an online mass spectrometer (MS) was used for the automated dosage of Cl_2. All the gaseous residues were neutralized in two interconnected concentrated KOH and Cu^{2+} solution-containing bottles. An active carbon-containing filter accounts of any remaining toxic gaseous intermediates.

Two different types of Cl_2 and CO detectors were placed under the fume hood to constantly monitor the Cl_2 and CO concentration at the work station. To avoid contamination with CO, two additional filters for CO entrapment were installed at the outlet of the six-port valve and of the reactor. The maximum amount of $COCl_2$ that could theoretically be formed in the pulse reactor (0.025 ppm) is lower than the permissible exposure limit (0.1 ppm averaged over a work shift of up to 10 h a day, 40 h per week with a ceiling level of 0.2 ppm averaged over a 15 min period).

Synthesis

Powder carbon synthesis

The sample indicated as CHT was obtained by dissolution of pure glucose in distilled water (180 mL) to form a clear solution, and placed in a Teflon-lined autoclave at 200 °C for 20 h. The product was then separated by filtration, washed several times with hot water, acetone, and ethanol. It was dried at 100 °C and further treated at 200 °C for 2 h. The quantitative yield was approximately 20 wt %.

Thermal annealing procedure

For each thermal annealing procedure, an amount of sample ($\approx$200 mg) was placed in a vertical fixed-bed reactor. The sample underwent graphitization at an annealing temperature of 1000 °C for 6 h under a bottom-up N_2-gas flow (100 STP mL min^{-1}). This sample is named CHT-tr.

Characterization

Carbon morphology structure was investigated by transmission electron microscopy (TEM) by using a Philips CM12 microscope (resolution 0.2 nm) equipped with a high-resolution camera, at an accelerating voltage of 120 kV. Suitable specimens for TEM analyses were prepared by ultrasonic dispersion in *iso*-propyl alcohol by adding a drop of the resulting suspension onto a holey carbon-supported grid.

Samples were characterized by X-ray powder diffraction (XRD) by using a Philips X-Pert diffractometer with a monochromatic $Cu_{K\alpha}$ ($\lambda = 1.54056$ Å) radiation at 40 kV and 30 mA. Data were collected over a 2θ range of 10–100 degrees, with a step size of 0.04° at a time per step of 3 s. The graphitization degree of onion-like carbon nanospheres was quantitatively determined by using LiF as a standard material (in a ratio from 1 to 5). For quantification, the peak area and the intensity were used and analyzed comparatively to the standard sample. Results are presented in Table 1 and shown in Figure S1.

The specific surface areas were calculated by using the Brunauer Emmett Teller (BET) equation from the adsorption branch of the isotherms, obtained at -196 °C on a Quantachrome sorption analyser. Prior to the measurements, samples were heated in a N_2 flow at 350 °C for 1 h. The micropore volume was evaluated by the t-plot method.

X-ray Photoelectron Spectroscopy (XPS) data were measured by using a Physical Electronics GMBH PHI 5800-01 spectrometer operating with a monochromatized $Al_{K\alpha}$ radiation with a power beam of 300 W. The pass energy for determination of the oxidation state and concentration of surface species was 11.0 and 58.0 eV, respectively. The BE regions of C_{1s} (280–300 eV) and O_{1s} (524–544 eV) were investigated, taking the Al_{2p} line (73.0 eV) of aluminum standard as a reference for signal calibration. Ar^+ 2 kW voltage small beam sputtering was performed to remove adventurous carbon.

Raman spectra at 514 nm (2.41 eV, Ar^+ laser) were recorded with a Renishaw (Series 1000) spectrometer equipped with a 50× objective. All Raman spectra were obtained following the thermal activation of the carbon materials under inert conditions at 150 °C for 1 h. After Cl_2 treatment further measurements under inert conditions (in N_2 flow) were performed. For in situ Raman measurements a temperature-regulated quartz reactor (1.62 mm internal diameter) was used.

Activity tests

Multipulse experiments were carried out to investigate the interactions of the carbon materials with Cl_2 and to identify the transiently formed intermediates when reacting with CO and CH_4. For each experiment, the solid carbon material (10 mg, particle size $\leq$80 μm) packed in a quartz reactor (0.4 cm internal diameter) was activated in He flow (10 mL min^{-1}) at 150 °C for 1 h prior to catalysis. The schematic representation of the experimental setup constructed for the Cl_2 activation study is shown in the Supporting Information, Figure S2. Multiple Cl_2 pulses (3.6 μmol Cl_2/pulse, pulse length 230 s) were performed to understand the catalytic activation of Cl_2 on the multiple active sites in the selected carbons. To probe the nature of activated Cl_2 species in separate experiments, 5 % CO and CH_4 in He carrier (flow rate 10 mL min^{-1}) were exposed to the Cl-containing carbon sample. All gaseous products were analyzed by online mass spectrometry (PFEIFFER OMNIstar/TM mass-spectrometer, QMS 200). For the identification of the surface-bound species, temperature-programmed desorption (TPD) was performed up to 800 °C with a temperature increment of 5 °C min^{-1} in He flow (flow rate 10 mL min^{-1}).

Acknowledgements

The authors acknowledge support from the European Community's Seventh Framework Program [FP7/2007–2013] under grant agreement no. NMP-LA-2010–245988 (INCAS).

Keywords: carbon · chlorination · graphene · nanostructures · strained molecules

[1] a) Y. Qin, L. He, J. Duan, P. Chen, H. Lou, X. Zheng, H. Hong, *ChemCatChem* **2014**, *6*, 2698; b) V. Calvino-Casilda, A. J. Lopez-Peinado, C. J. Duran-Valle, R. M. Martin-Aranda, *Catal. Rev. Sci. Eng.* **2010**, *52*, 325; c) T. J. Bandosz in *Carbon Materials for Catalysis* (Eds.: P. Serp, J. L. Figueiredo), Wiley, Hoboken, **2008**, p. 45.

[2] a) W. Qi, D. Su, *ACS Catal.* **2014**, *4*, 3212; b) D. C. Sorescu, K. D. Jordan, P. Avouris, *J. Phys. Chem. B* **2001**, *105*, 11227; c) Z. Y. Zhu, S. M. Lee, Y. H. Lee, T. Frauenheim, *Phys. Rev. Lett.* **2000**, *85*, 2757; d) J. Zhang, X. Liu, R. Blume, Z. Zhang, R. Schlögl, D. Su, *Science* **2008**, *322*, 73.

[3] a) D. S. Su, G. Centi, S. Perathoner, *Chem. Rev.* **2013**, *113*, 5782; b) G. Centi, S. Perathoner, D. S. Su, *Catal. Surv. Asia* **2014**, *18*, 149; c) D. S. Su, G. Centi, S. Perathoner, *Catal. Today* **2012**, *186*, 1.

[4] a) J. H. Bitter, *J. Mater. Chem.* **2010**, *20*, 7312; b) X. Pan, X. Bao, *Acc. Chem. Res.* **2011**, *44*, 553.

[5] R. Arrigo, M. Hävecker, S. Wrabetz, R. Blume, M. Lerch, J. McGregor, E. P. J. Parrott, J. A. Zeitler, L. F. Gladden, A. Knop-Gericke, R. Schlögl, D. S. Su, *J. Am. Chem. Soc.* **2010**, *132*, 9616–9630.

[6] L. Mleczko, G. Lolli, *Angew. Chem. Int. Ed.* **2013**, *52*, 9372–9387; *Angew. Chem.* **2013**, *125*, 9540–9557.

[7] J.-W. Shi, X. Zong, X. Wu, H.-J. Cui, B. Xu, L. Wang, M.-L. Fu, *ChemCatChem* **2012**, *4*, 488–491.

[8] D. S. Su, J. Zhang, B. Frank, A. Thomas, X. Wang, J. Paraknowitsch, R. Schlögl, *ChemSusChem* **2010**, *3*, 136.

[9] R. Chakravarti, M. L. Kantam, H. Iwai, S. S. Al-deyab, K. Ariga, D.-H. Park, J.-H. Choy, K. S. Lakhi, A. Vinu, *ChemCatChem* **2014**, *6*, 2872.

[10] D. S. Su, J.-O. Müller, R. E. Jentoft, D. Rothe, E. Jacob, R. Schlögl, *Top. Catal.* **2004**, *30–31*, 241.

© 2015 Wiley-VCH Verlag GmbH & Co. KGaA, Weinheim

[11] V. Georgakilas, J. A. Perman, J. Tucek, R. Zboril, *Chem. Rev.* **2015**, *115*, 4744.
[12] T. J. Bandosz, M. Seredych, *Chin. J. Catal.* **2014**, *35*, 807.
[13] J. Matthiesen, T. Hoff, C. Liu, C. Pueschel, R. Rao, J.-P. Tessonnier, *Chin. J. Catal.* **2014**, *35*, 842.
[14] L. R. Radovic, C. Mora-Vilches, A. J. A. Salgado-Casanova, *Chin. J. Catal.* **2014**, *35*, 792.
[15] G. Centi, S. Perathoner, *ChemSusChem* **2011**, *4*, 913.
[16] M. Godino-Ojer, A. J. López-Peinado, R. M. Martín-Aranda, J. Przepiórski, E. Pérez-Mayoral, E. Soriano, *ChemCatChem* **2014**, *6*, 3440.
[17] W. Zhang, L. Theil Kuhn, *ChemCatChem* **2013**, *5*, 2591.
[18] Y. Zhu, Y. Lin, B. Zhang, J. Rong, B. Zong, D. S. Su, *ChemCatChem* **2015**, DOI: 10.1002/cctc.201402930.
[19] R. Wang, X. Sun, B. Zhang, X. Sun, D. Su, *Chem. Eur. J.* **2014**, *20*, 6324.
[20] J. Zhu, A. Holmen, D. Chen, *ChemCatChem* **2013**, *5*, 378.
[21] A. Ramos, I. Cameán, A. B. García, *Carbon* **2013**, *59*, 2-32.
[22] D. Tasis, N. Tagmatarchis, A. Bianco, M. Prato, *Chem. Rev.* **2006**, *106*, 1105.
[23] C. T. J. Low, F. C. Walsh, M. H. Chakrabarti, M. A. Hashim, M. A. Hussain, *Carbon* **2013**, *54*, 1.
[24] S. Stankovich, D. A. Dikin, R. D. Piner, K. A. Kohlhaas, A. Kleinhammes, Y. Jia, Y. Wu, S. T. Nguyen, R. S. Ruoff, *Carbon* **2007**, *45*, 1558.
[25] S. Y. Sawant, R. S. Somani, A. B. Panda, H. C. Bajaj, *Mater. Lett.* **2013**, *94*, 132.
[26] D. R. Dreyer, H.-P. Jia, C. W. Bielawski, *Angew. Chem. Int. Ed.* **2010**, *49*, 6813; *Angew. Chem.* **2010**, *122*, 6965.
[27] Y. Z. Jin, C. Gao, W. K. Hsu, Y. Zhu, A. Huczko, M. Bystrzejewski, M. Roe, C. Y. Lee, S. Acquah, H. Kroto, D. R. M. Walton, *Carbon* **2005**, *43*, 1944.
[28] C. Su, K. P. Loh, *Acc. Chem. Res.* **2013**, *46*, 2275.
[29] B. Keggenhoff, H. Lokum, J. Münnig, *Process and apparatus for the production of phosgene*, Patent US7442835, **2008**.
[30] C. J. Mitchell, K. S. van der Velde, M. Smit, R. Scheringa, K. Ahrika, D. H. Jones, *Catal. Sci. Technol.* **2012**, *2*, 2109.
[31] J.-P. Senet, *C. R. Acad. Sci. Ser. IIc: Chim.* **2000**, *3*, 505.
[32] L. Cotarca, H. Eckert, *Phosgenations—A Handbook*, Wiley-VCH, Weinheim, **2005**.
[33] V. A. Volodina, A. A. Kozlovskii, S. I. Kuzina, A. I. Mikhailov, *High Energy Chem.* **2008**, *42*, 311.
[34] T. Zhang, C. Troll, B. Rieger, J. Kintrup, O. F. K. Schlüter, R. Weber, *J. Catal.* **2010**, *270*, 76.
[35] J. Heuser, H. Kauth, C. Kords, *Phosgene having low content of carbon tetrachloride*, Patent US6930202, **2005**.
[36] F. A. Via, G. L. Soloveichlk, P. G. Kosky, W. V. Cicha, *Method for producing phosgene*, Patent US6500984, **2002**.
[37] H. Şahin, S. Ciraci, *J. Phys. Chem. C* **2012**, *116*, 24075.
[38] B. Li, L. Zhou, D. Wu, H. Peng, K. Yan, Y. Zhou, Z. Liu, *ACS Nano* **2011**, *5*, 5957.
[39] K. Gopalakrishnan, K. S. Subrahmanyam, P. Kumar, A. Govindaraj, C. N. R. Rao, *RSC Adv.* **2012**, *2*, 1605.
[40] M. Yang, L. Zhou, J. Wang, Z. Liu, Z. Liu, *J. Phys. Chem. C* **2012**, *116*, 844.
[41] S. Abate, G. Centi, S. Perathoner, *Natl. Sci. Rev.* **2015**, *2*, 143.
[42] I. M. Y. A. M. Rabiu, *J. Power Energy Eng.* **2013**, *1*, 41.
[43] C. Hammond, S. Conrad, I. Hermans, *ChemSusChem* **2012**, *5*, 1668.
[44] Y. Wei, D. Zhang, Z. Liu, B.-L. Su, *Cuihua Xuebao* **2012**, *33*, 11.
[45] Z. Guo, B. Liu, Q. Zhang, W. Deng, Y. Wang, Y. Yang, *Chem. Soc. Rev.* **2014**, *43*, 3480.
[46] J. He, T. Xu, Z. Wang, Q. Zhang, W. Deng, Y. Wang, *Angew. Chem. Int. Ed.* **2012**, *51*, 2438; *Angew. Chem.* **2012**, *124*, 2488.
[47] K. Barbera, L. Frusteri, G. Italiano, L. Spadaro, F. Frusteri, S. Perathoner, G. Centi, *Chin. J. Catal.* **2014**, *35*, 869.
[48] L. Frusteri, C. Cannilla, K. Barbera, S. Perathoner, G. Centi, F. Frusteri, *Carbon* **2013**, *59*, 296.
[49] X.-Y. Liu, J.-M. Zhang, K.-W. Xu, *Physica B* **2014**, *436*, 54.
[50] J. Zhang, D. S. Su, R. Blume, R. Schlögl, R. Wang, X. Yang, A. Gajovic, *Angew. Chem. Int. Ed.* **2010**, *49*, 8640; *Angew. Chem.* **2010**, *122*, 8822.
[51] Z. Wang, L. Yu, W. Zhang, Z. Zhu, G. He, Y. Chen, G. Hu, *Phys. Lett. A* **2003**, *307*, 249–252.
[52] W. Zhang, M. Yao, X. Fan, S. Zhao, S. Chen, C. Gong, Y. Yuan, R. Liu, B. Liu, *J. Chem. Phys.* **2015**, *142*, 034702.
[53] a) J. Robertson, *Phys. Rev. B* **2000**, *61*, 14095; b) S. E. Rodil, J. Robertson, *Phys. Rev. B* **2003**, *67*, 155306.
[54] P. K. Chu, L. Li, *Mater. Chem. Phys.* **2006**, *96*, 253.
[55] N. A. Marks, D. W. M. La, *Phys. Rev. B* **2009**, *79*, 075430.
[56] A. C. Ferrari, *Solid State Commun.* **2007**, *143*, 47.
[57] J. Shang, L. Ma, J. Li, W. Ai, T. Yu, G. G. Gurzadyan, *Sci. Rep.* **2012**, *2*, 792.
[58] F. Tuinstra, J. L. Koening, *J. Chem. Phys.* **1970**, *53*, 1126.
[59] D. Nishide, H. Kataura, S. Suzuki, K. Tsukagoshi, Y. Aoyagi, Y. Achiba, *Chem. Phys. Lett.* **2003**, *372*, 45.
[60] V. M. Irurzun, M. Pilar Ruiz, D. E. Resasco, *Carbon* **2010**, *48*, 2873.
[61] S. Yumitori, *J. Mater. Sci.* **2000**, *35*, 139.
[62] Y. Ling, G. K. Koyanagi, D. Caraiman, V. Baranov, D. K. Bohme, *Int. J. Mass Spectrom.* **1999**, *182/183*, 349.
[63] I.-Y. Jeon, H. M. Kim, I. T. Choi, K. Lim, J. Ko, J. C. Kim, H.-J. Choi, M. J. Ju, J.-J. Lee, H. K. Kim, *Nano Energy* **2015**, *13*, 336.
[64] G. Czakó, J. M. Bowman, *J. Chem. Phys.* **2012**, *136*, 044307/1.
[65] Z. Chen, W. Thiel, A. Hirsch, *ChemPhysChem* **2003**, *4*, 93.
[66] I. H. Campbell, D. L. Smith, *Solid State Physics 55* (Eds.: H. Ehrenreich, F.Spaepen), Academic Press, New York, **2000**.
[67] P. A. van Hal, M. P. T. Christiaans, M. M. Wienk, J. M. Kroon, R. A. J. Janssen, *Phys. Rev. B* **1999**, *103*, 4352.

Received: June 10, 2015
Revised: July 29, 2015
Published online on August 31, 2015

© 2015 Wiley-VCH Verlag GmbH & Co. KGaA, Weinheim